

A Novel Strategy for the Application of an Oxide Layer to the Front Interface of Cu(In,Ga)Se₂ Thin Film Solar Cells: Al₂O₃/HfO₂ Multi-Stack Design With Contact Openings

Peer-reviewed author version

BULDU KOHL, Dilara; DE WILD, Jessica; KOHL, Thierry; BIRANT, Gizem; BRAMMERTZ, Guy; MEURIS, Marc; POORTMANS, Jef & VERMANG, Bart (2022) A Novel Strategy for the Application of an Oxide Layer to the Front Interface of Cu(In,Ga)Se₂ Thin Film Solar Cells: Al₂O₃/HfO₂ Multi-Stack Design With Contact Openings. In: IEEE Journal of Photovoltaics, 12 (1) , p. 301 -308.

DOI: 10.1109/JPHOTOV.2021.3120515

Handle: <http://hdl.handle.net/1942/36398>

A novel strategy for the application of an oxide layer to the front interface of Cu(In,Ga)Se₂ thin film solar cells: Al₂O₃/HfO₂ multi-stack design with contact openings

Dilara G. Buldu, Jessica de Wild, Thierry Kohl, Gizem Birant, Guy Brammertz, Marc Meuris, Jef Poortmans, Bart Vermang

Abstract— Interface recombination is one of the factors limiting the performance of Cu(In,Ga)Se₂ (CIGS). Especially in the absence of band grading at the front and rear surface, interface passivation approaches become important to improve device performance. The integration of an oxide layer as passivation layer at the front surface of the CIGS requires meticulous considerations in order not to impact the further steps of the solar cell production. In this work, a novel approach is reported to try to tackle the problem of interface recombination at the front surface of CIGS without affecting further solar cell production steps. In this approach a Al₂O₃/HfO₂ multi-stack layer with contact openings is applied. NaCl template patterning with preliminarily selected parameters was used to create a homogeneous pattern of contact opening on the CIGS surface and allow the current flow in the device. After the removal of the NaCl islands, the holes in the multi-stack (openings) were visualized by scanning electron microscopy. In addition, energy-dispersive X-ray spectroscopy (EDS) was performed before and after chemical bath deposition of the buffer layer. The EDS result confirmed that the undesired etching of the Al₂O₃ layer during buffer layer deposition was prevented by using a thin HfO₂ layer. Solar cells were produced by using preliminarily selected parameters for the multi-stack design. As a result, without having a significant negative impact on the solar cell parameters, a device design was achieved which is almost comparable with the reference device. In addition, options for future improvement and development are discussed.

Index Terms— Al₂O₃, contact openings, Cu(In,Ga)Se₂ (CIGS) solar cells, HfO₂, multi-stack, front interface.

I. INTRODUCTION

THE absorber material Cu(In,Ga)Se₂ (CIGS) is one of the most promising materials in the field of thin-film photovoltaic (PV) technologies due to its potential for building

integrated PV as well as its high conversion efficiencies of up to 23.35% [1]. This world record efficiency was achieved with heavy alkali post deposition treatment and a Cd-free buffer layer on band gap graded CIGS. However, CIGS is still suffering from the low open-circuit voltage (V_{oc}) [2]. A recent study suggested that the use of ungraded CIGS instead of a graded one can provide simple and better understanding to tackle this problem [3]. Mostly, the V_{oc} losses come from non-radiative recombination in the bulk and recombination at rear/front interfaces. The solution for these losses is either to improve the quality of the CIGS material or a better interface engineering. Indeed, the rear and front interfaces become more important in the absence of band grading. One way to tackle these drawbacks is to implement a passivation layer at the rear/front interface. Doing this on the ungraded CIGS could bring a clear understanding of the effect of the surface passivation since the effect of applied surface passivation can potentially be overshadowed in the presence of band grading. Over the years, surface passivation has been applied in Si-based technology using different passivation materials such as Al₂O₃, HfO₂ and SiO₂ [4]. Even though this concept is well known and used in Si-based technology, we can say that it is in a very early stage of development for CIGS solar cells. In the last decade, the concept of a passivation layer with contact openings has been implemented at the rear surface of CIGS using various passivation materials and different approaches to create contact openings [5]–[8]. However, the same thing cannot be said for the front surface, since only a limited number of attempts have been made to apply this concept at the CIGS/buffer interface. Simulation-based studies showed that the implementation of a passivation layer with contact openings at the CIGS/buffer layer interface can have beneficial effect on the V_{oc} and the device performance [9], [10]. Nevertheless, the improvement in

Manuscript received June 2021. This work received funding from the European Union's H2020 research and innovation program under grant agreement No. 715027.

D. G. Buldu, J. de Wild, T. Kohl, G. Birant, G. Brammertz, M. Meuris, J. Poortmans and B. Vermang are with the Institute for Material Research (IMO) Hasselt University (partner in Solliance), Wetenschapspark 1, 3590 Diepenbeek, Belgium and with Imec division IMOMECE(partner in Solliance), Wetenschapspark 1, Diepenbeek 3590, Belgium and with Energyville, Thor Park Genk 8320, Genk 3600, Belgium

(e-mail: dilara.gokcen.buldu@imec.be; jessica.dewild@imec.be; thierry.kohl@imec.be; gizem.birant@imec.be; guy.brammertz@imec.be; marc.meuris@imec.be; bart.vermang@imec.be) J. Poortmans is with imec, Kapeldreef 75, 3001 Leuven, Belgium (e-mail: jef.poortmans@imec.be). J. Poortmans is also with the Department of Electrical Engineering, KU Leuven, Kasteelpark Arenberg 10, 3001 Heverlee, Belgium.

the device performance is strongly dependent on the size and distribution of the contact openings [9], [10]. So far, a few studies showed the use of different passivation layers and their impacts. The use of Al_2O_3 was reported for the first time by Hsu et al. and it was shown that the passivation effect is visible even with a thin layer on the CIGS [11]. A thin GaO_x layer was used as a passivation layer and the device performance was improved after the layer implementation between CIGS and buffer layer interface [12]. Moreover, a few studies showed the implementation of the passivation layer with contact openings. In one of the studies, silica nanosphere lithography was used to create the contact in the Al_2O_3 layer. Even though Al_2O_3 improved the device performance compared to a ZnO buffer layer, the device performance was lower compared to CdS buffer layer [13]. In another study, the pattern for contacts was formed by using a NaCl alkali solution on CIGS and a HfO_2 layer was deposited on this pattern. Although the use of NaCl alkali solution is simpler than other methods, the device performance was not significantly changed compared to the reference sample [14]. Even if both studies demonstrated promising methods to create contact openings in an oxide layer and the implementation of these techniques for CIGS solar cells, a significant improvement in V_{oc} or device performance was not shown.

In light of the former reported work, in this contribution, we suggest a new strategy for the front surface passivation of CIGS by applying a multi-stack passivation layer with contact openings. The use of stack passivation layers is common for Si-based technology [15]. The aim behind this approach is to maintain an interface between a desirable oxide with good surface passivation properties and the absorber. As an example, Al_2O_3 is a promising material for the passivation of CIGS interfaces [11], [16], [17]. However, the Al_2O_3 layer is not compatible with further solar cell production steps since it is not chemically resistant to ammonia-based solutions [18] i.e. the ones used in typical chemical bath deposition for buffer layers. Therefore, we propose to apply a second layer such as HfO_2 which is chemically resistant to such conditions [14]. In this manner, the bottom layer, in this case Al_2O_3 , can be protected during the chemical bath deposition and this multi-stack design is compatible for further steps of solar cell production.

II. EXPERIMENTAL METHOD

A. Solar Cell Production

The CIGS layer was deposited by using a simple one-stage co-evaporation method on a SLG substrate which is covered with a Si(O,N) alkali diffusion barrier and with a Mo back contact. The evaporation rate for all sources was kept constant during the deposition until the desired thickness was reached. The final thickness of the absorber is 1.6 μm . With this process, a flat and homogenous Ga profile was achieved [19]. The composition of the absorber layer was measured by X-ray fluorescence (XRF). The $\text{Cu}/(\text{Ga}+\text{In})$ ratio is around 0.77-0.8 and $\text{Ga}/(\text{Ga}+\text{In})$ is around 0.3. An ammonium sulfide ($(\text{NH}_4)_2\text{S}$) solution with 6-7.5% sulfur concentration was used for surface

treatment as described in our previous work [20]. A similar study with an ammonium hydroxide pre-cleaning step instead of ammonium sulfide was presented at the IEEE Photovoltaic Specialist Conference [21].

The pattern for the contact openings was created using a NaCl solution as proposed by Löckinger et al. [14]. The parameters of the solution were updated for our process. Samples were dipped in the 0.5M NaCl solution for 90 second at 50 °C. Then, Al_2O_3 and HfO_2 layers were deposited via atomic layer deposition (ALD) at 300 °C and 250 °C, respectively. Trimethylaluminium (TMA) and Tetrakis-EthylMethylAmino Hafnium (TEMAH) were used as a precursor for Al_2O_3 and HfO_2 , respectively, and H_2O was used as a reactant. A 8 nm thick Al_2O_3 layer was deposited with a growth rate 0.17nm/cycle and a 2 nm HfO_2 layer was deposited with a growth rate 0.14nm/cycle. Then, the samples were cleaned in an ultrasonic water bath until all the salts dissolved. This dissolution was typically timed to be around 15 min. At the end of this process, the NaCl salt islands were removed and left holes, i.e openings, in the multi-stack oxide layers.

Two samples were prepared to compare with the multi-stack design. The first sample was the reference sample (REF), and it was directly processed for solar cells after the ammonium sulfide surface treatment. The second sample was used to clearly distinguish the impact of the NaCl pattern from the multi-stack passivation, since alkali elements have beneficial impact and improve electronic properties of CIGS solar cells [22]. The NaCl pattern was created on CIGS layer after the ammonium sulfide surface treatment and then the sample was annealed for 35 min at 300 °C under N_2 atmosphere in the oven. This way, the ALD anneal process that is used for multi-stack design was mimicked for this sample. This sample will be referred to as Pattern Anneal (PA) sample in the text. An overview of the samples processing, and its illustration is shown in Fig. 1. For the solar cell production, a CdS buffer layer was deposited at 65 °C by chemical bath deposition. The aqueous solution was prepared with cadmium acetate dihydrate (2.7M), thiourea (95mM) and ammonium hydroxide (2M), and the deposition took around 12-13min. In addition, it was observed in our preliminary work that the CdS formation on CIGS and HfO_2 is different. Indeed, CdS typically seems to deposit less (thinner) on the HfO_2 surface as compared to CIGS surface (Fig. S1a). Therefore, one more CdS deposition was done for the multi-stack design, by doing so we can exclude the reduced thickness of CdS as a parameter in further analysis (Fig. S2). Solar cells were finished with (60nm) i-ZnO/(150nm) ITO and Ni/Ag grids.

B. Characterization

The pattern and the contact openings were visualized with scanning electron microscopy (SEM) on a Tescan Vega3. To make sure that the Al_2O_3 layer is still present after the buffer layer deposition, energy dispersive X-ray spectroscopy (EDS) was performed. **To be surface sensitive, the EDS measurement was performed at 7kV with 14 beam intensity and a 300nm spot size. These parameters were kept constant for each EDS measurement.** Photoluminescence (PL) and time-resolved

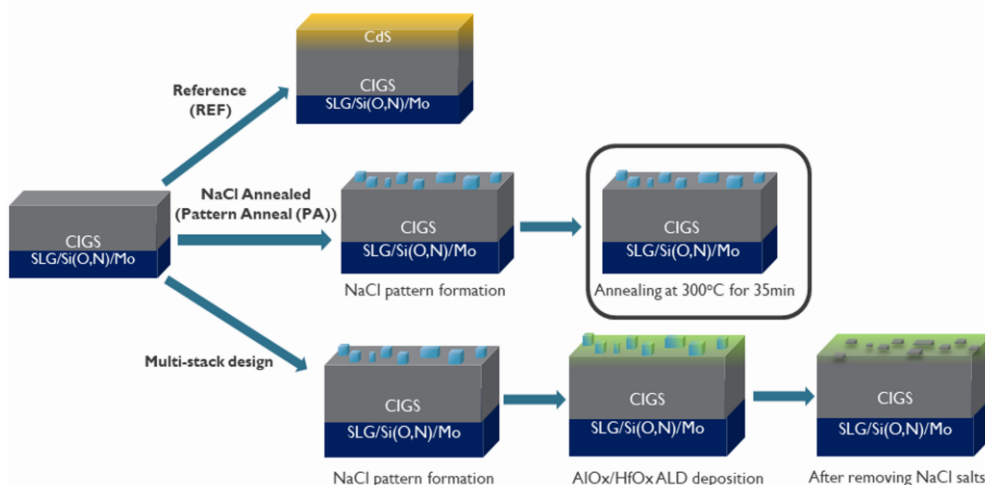


Fig. 1. Schematic representation of the different samples and their additional steps before the solar cell production

photoluminescence (TRPL) measurements were performed with a Picoquant FluTime 300 system with a 532 nm excitation wavelength, time resolution of 25ps and a repetition rate of 3MHz. Samples were $2.5 \times 5 \text{ cm}^2$, and the cells of 0.5 cm^2 were mechanically scribed. 10-12 cells in the finished solar cells were characterized with current-voltage (JV) measurements with a Keithley 2400 source meter and four terminal sensing under 1000 W/m^2 , A.M 1.5 at room temperature. External quantum efficiency (EQE) was measured under dark condition and under light bias condition and scanned from 350nm to 1300nm with 10nm steps. Capacitance-Voltage measurements were performed using an Agilent Precision LCR meter. The solar cells were measured at room temperature and a frequency of 100kHz with a DC bias range from -2.5V to 1V with 0.1V steps.

III. RESULT AND DISCUSSION

A. Design of the multi-stack with contact openings and Characterization

When Al_2O_3 is added at the front surface of CIGS, the solar cell production requires adaptation. For example, when conventional chemical bath deposition is used to deposit CdS on the Al_2O_3 layer, it is etched during this process [17]. However, even when other conventional methods, such as sputtering or ALD, are used to deposit the buffer layer, the device with Al_2O_3 shows lower performance than the reference devices [23]. Prior to designing the multi-stack structure, we investigated the etching of our Al_2O_3 layer by depositing a thick layer (10nm) on NaCl/CIGS surface and submitting it to the chemical bath environment. The change of the surface morphology from oxide layer deposition on NaCl/CIGS to end of the buffer layer deposition can be seen in Fig. 2. When the SEM images before and after ultrasonic wash are compared, it can be seen that the NaCl islands leave holes in the Al_2O_3 . After the buffer layer deposition, the pattern was no longer visible (see in Fig. 2(c)). This was the first indication that our Al_2O_3 layer is etched during the CdS deposition. In addition, the EDS result showed that the detected O level differs after each step. Before ultrasonic wash step, 15% O was detected on the

surface. After the ultrasonic wash (Fig. 2(b)), the dark spots exhibit 1.5% O level while the rest of the surface showed 15% O level similar to the case before the ultrasonic wash step. This indicates that the NaCl islands dissolved successfully and left holes in the oxide layer. However, after the buffer layer deposition, the detected O level on the surface was 2%. Thus, the Al_2O_3 layer is not chemically resistant to the conventional buffer layer deposition.

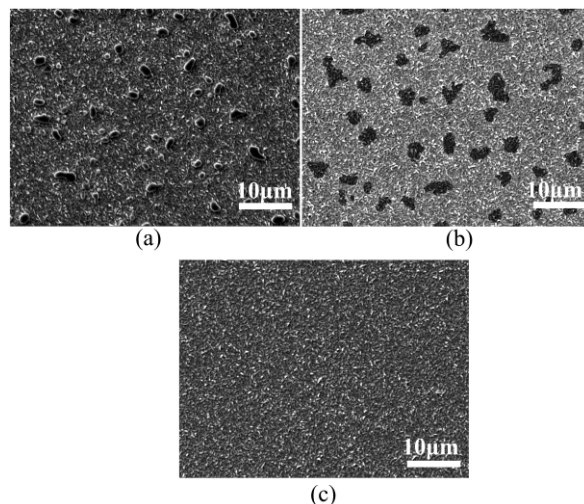


Fig. 2. SE micrograph of the SLG/SiO_x/Mo/CIGS/NaCl pattern/ Al_2O_3 sample. (a) Before ultrasonic wash, (b) after ultrasonic wash (15min). Dark spots are the created openings after the dissolution of the NaCl islands. (c) After the CdS buffer layer deposition. The pattern of the contact openings was disappeared due to etching of the Al_2O_3 layer.

To protect the Al_2O_3 layer, we applied a thin HfO_2 cap, which is chemically resistant to ammonia-based solutions. The NaCl pattern before the creation of openings i.e. before the ultrasonic bath washing can be seen in Fig. 3(a). During the ultrasonic washing process, the NaCl salts dissolved in the water leaving holes in the oxide layers behind, see dark spots in Fig. 3(b). These holes in the multi-stack layer later served as contact openings for the sample. After this step, the buffer layer was deposited on the multi-stack structure. The pattern of contact openings remained almost unaffected by the buffer layer

deposition, see in Fig. 3(c). This was the first indication that a thin HfO_2 layer can protect the Al_2O_3 during the buffer layer deposition which includes ammonium-hydroxide. **The performance of the device is strongly dependent on opening size and distribution. As it can be seen in Fig. 3(b), the holes (dark spots) are random and do not have a well-defined shape. Therefore, to avoid a high error margin three different SE micrographs were used to extract the surface coverage of the oxide, the distance between two openings, and their sizes. As a result, an area of contact openings of 8-10% was found, i.e. a surface coverage for the oxide layers of 90-92%. The size of the openings changed from 1-3 μm and the distance between two openings fluctuated from 1-6 μm .** Detailed EDS measurements were performed before and after the ultrasonic bath washing to verify that all NaCl salts were removed from the surface and to distinguish between the openings and multi-stack layer. In

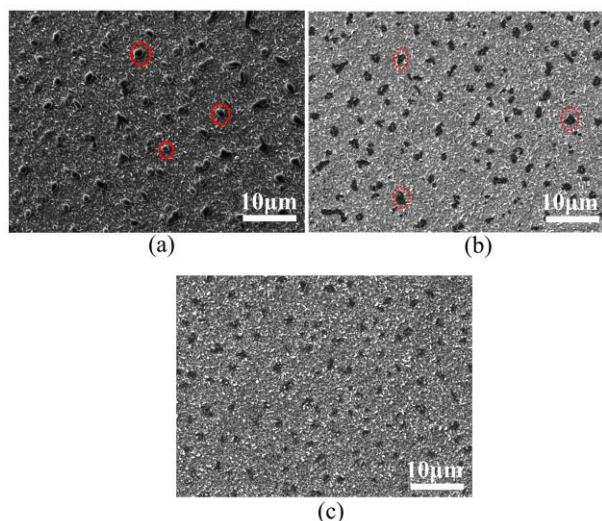


Fig. 3. SE micrographs for multi-stack design. (a) Before ultrasonic bath wash. An NaCl salt is highlighted with a red circle. (b) After ultrasonic bath wash (15min). The dark spots show the holes where the salts were removed (red dashed line circle). (c) After CdS deposition. The pattern was not damaged by CBD deposition which includes ammonium hydroxide solution.

addition, one more EDS measurement was performed after buffer layer deposition to assure that the undesired Al_2O_3 etching was prevented. The average of the atomic percentage of specific elements, such as Al, Hf, and O for the multi-stack layer and Na and Cl for the salt islands, were extracted from EDS measurement and can be seen in Fig.4. The first observation was that the oxide layers were grown selectively on the CIGS/NaCl surface. In other words, the oxide layers were deposited thinner on the NaCl salt surface as compared to the CIGS surface. This can be seen in Fig. 4(a) since the atomic percentage of Al, Hf, and O were almost two times lower on the salts surface. When the measurements before and after ultrasonic bath wash are compared, it can be said that NaCl islands were mostly removed from the surface. Neither of the Na, Cl, Al and Hf elements were detected in the regions where the holes formed. This means that, while the salts were dissolving in the water, the oxide layers on them were also removed. In addition, the oxygen level was higher on the layer as compared to the holes. Furthermore, it can be deduced that

the multi-stack layer remained almost undamaged after the ultrasonic bath because the atomic percentage of Al, Hf, and O elements remains almost unchanged. At this point, it can be said that the contact openings were created in the multi-stack layer successfully.

The buffer layer deposition was done on this sample to create the p/n junction through the contact openings. Earlier, it was reported that CdS formation is improper on HfO_2 [14]. We also observed that the CdS layer formation on the HfO_2 surface was different than on the CIGS surface (in the openings), see in Fig. S1(a). The formation of CdS in the openings (the CIGS surface) was similar to the REF and PA samples after the first buffer layer deposition, however, lower amounts of Cd and S were detected on the multi-stack layer (HfO_2 surface), see Fig S1(b). Even though the CdS layer on the multi-stack (HfO_2 surface) is

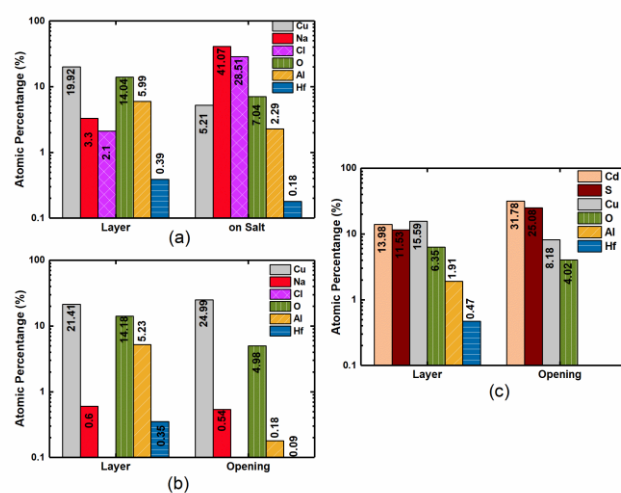


Fig. 4. Atomic percentage as extracted from EDX results. (a) Before ultrasonic wash and (b) after the ultrasonic bath wash. The holes were created by removing the salts in the multi-stack layer. (c) After CdS deposition. The aluminum layer was protected with hafnium layer in the multi-stack layer area.

unnecessary for the p/n junction, for the sake of comparability of all samples, a second buffer layer deposition was done to equalize the CdS layer on all samples. After the buffer layer depositions, non-negligible amounts of Al, Hf and O were detected **on the layer**, see in Fig 4(c), meaning that Al_2O_3 and HfO_2 layer were able to withstand this process. Since we can still detect Hf, Al, and O in non-negligible amounts and that the overall shape of our pattern did not change, we conclude that the Al_2O_3 layer was successfully protected from the chemical bath environment by the addition of a HfO_2 layer. **We believe that the O detected in the openings is not directly related to the oxide layer since the PA and reference sample also show an O signal after CdS deposition (see Fig. S1(b)). This could be due to contamination during the CdS deposition and/or after the deposition.**

To investigate the effect of the multi-stack design, PL and TRPL measurements were performed on four different points on the samples. Both measurements are an effective way to probe the interface and study effect of the multi-stack layer. The change of the PL intensity was investigated after each additional step e.g after annealing for the PA sample or after

implementation of oxide layers for the multi-stack sample. The change in the PL intensity was given as ratio from bare (as-deposited) CIGS to CdS covered CIGS in Fig. 5(a). Firstly, the PL intensity is doubled following the CdS deposition for the REF sample. This improvement can be expected due to the well-known **beneficial** effect of CdS[24]. For the PA sample, a slight improvement was observed after annealing, however, the overall improvement was almost the same as for the REF sample. The PL intensity was further improved by adding the multi-stack oxide layer. In addition, the PL decay time was slightly improved with the multi-stack design compared to the REF and PA sample (Fig 5(b)). **Only the graphical improvement in the PL decay time was taken into account since our samples have a, on average, low PL decay time (~1-2ns)** [19], [20]. Even though the improvement in PL decay time was minimal, a significant change (6x) in PL intensity was observed after application of the multi-stack oxide layers. This could be an indication of the reduced recombination at the front surface. Due to this comparison between PA and multi-stack sample, it can be said that the effect of the NaCl pattern on the improved PL intensity of the multi-stack sample is negligible and that most of the effect on the front surface is due to the oxide layers

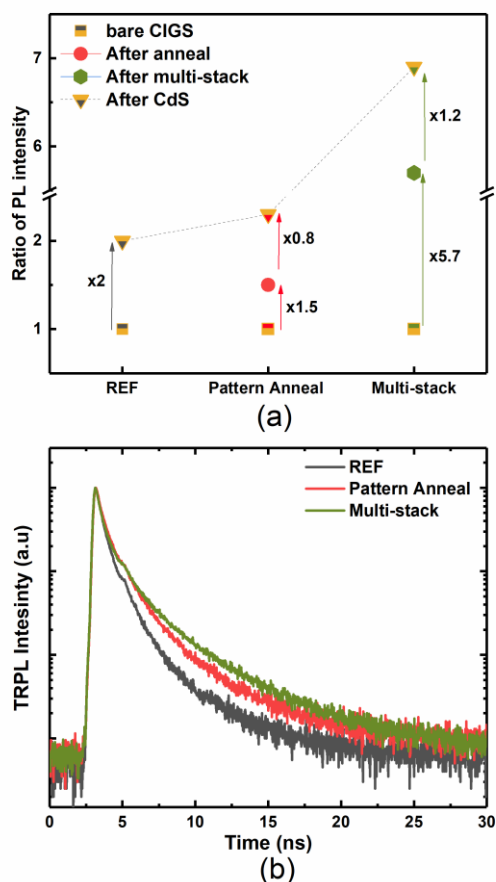


Fig. 5. (a) The PL intensity improvement was shown as ratio between bare CIGS (different colour square) and next process step (either after annealing (red dot) or after multi-stack layer deposition (green hexagon) and up to CdS deposition (different colour triangle). The improvement in PL intensity is higher with the multi-stack design. (b) The PL decay lifetime after buffer layer deposition for each sample.

themselves. At this point, it could be said that interface recombination may be reduced with the multi-stack design.

B. Electrical and Optical Characterization of Solar Cells

The already discussed improvements in both PL intensity and PL decay time of the multi-stack showed that it can be a promising candidate for solar cell applications. After these results, the samples were processed to solar cells. JV measurements were taken for ten cells on the samples and Fig. 6 shows the box plots of JV parameters. Generally, the V_{oc} increased with each additional step i.e pattern annealing or addition of the multi-stack, compared to the reference sample. While the improvement in V_{oc} for the PA sample is relatively small, a significant improvement was achieved with the addition of the multi-stack design. However, the FF slightly decreased with implementation of the multi-stack design. **Looking at the J-V curve of the device, could give an idea about the slight FF loss for the multi-stack design. As it can be seen in Fig. S3, the multi-stack design does not show any distortion (e.g. kink anomaly) that could typically be linked to a FF loss.**

As we mentioned before, the JV parameters strongly depend on the size of the contact openings and their distribution. Especially, the V_{oc} and FF are strongly affected by the contact openings pattern. While the size of the openings has significant effects to achieve high V_{oc} , the distance between the openings is much more important to achieve high FF[25]. In this case, we could say that while the size of the openings is good enough to have increased V_{oc} , the distribution of the openings, i.e distance between the openings, still needs to be optimized to achieve a higher FF for our contact openings pattern. Besides the contact opening pattern, the selected oxide layer properties play a role on JV parameters. For example, a material containing positive fixed charge density is mostly preferential for the passivation of the front surface of CIGS. The positive charges attract electrons (repels holes) at the surface and thus reduce the recombination as well as enhance photo-current flow[9]. In our case, our multi-stack design contains a negative fixed charge density[26]. This possibly leads to competing effects. While reducing the recombination at the interface by repelling electrons, the photo-current extraction could also be hindered. A current loss was observed for the PA sample which was increased for the multi-stack design. This J_{sc} loss is the main reason for the lower performance of the multi-stack design. **To understand the origin of the J_{sc} loss, EQE measurements were performed under dark and light bias condition, see Fig. 7. When the EQE response of the multi-stack sample was specifically examined, this sample showed overall lower EQE response as compared to the other samples. While the PA sample shows decreased carrier collection for the long wavelengths, the multi-stack sample suffers decreases in carrier collection in the long wavelength as well as in the short wavelength region. The additional slight reduction in the short wavelength indicates that the multi-stack sample has an additional carrier collection problem close to the interface. As we mentioned above, the properties of the oxide layer and the distance between the openings have significant impact on the device, which leads us to believe that the sub-optimal and negatively charged multi-stack design could be the**

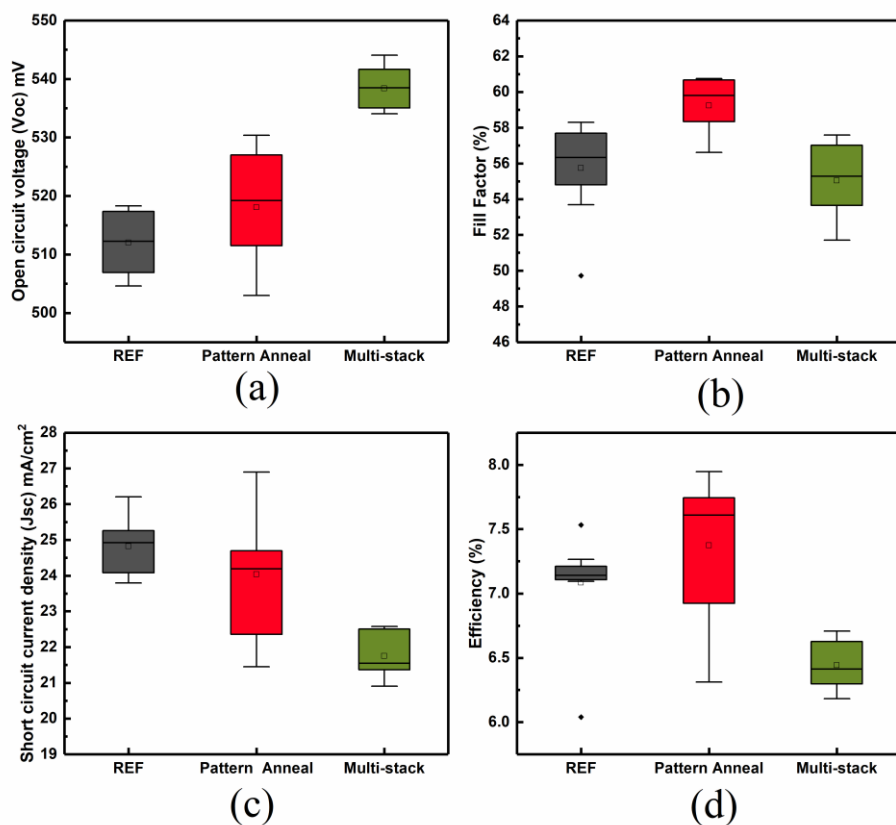


Fig. 6. JV parameter comparison between reference samples and multi-stack design. (a) Voc, (b) Fill Factor, (c) Jsc, and (d) Efficiency

reason for this observation. However, it can be seen that the EQE curve of both the PA and the multi-stack design samples are more heavily inclined towards the long-wavelength region as compared to the REF. This observed drop at long-wavelengths for both the PA and multi-stack design sample indicates that the multi-stack with sub-optimal contact openings is not the only reason for the changes in EQE behavior, since the NaCl pattern itself also has a negative impact on the EQE response at longer wavelengths. Furthermore, the EQE measurement was performed under light bias condition and while REF and PA samples show similar EQE response as in the dark, a slight increase was observed in the long-wavelength region for the multi-stack sample, see in Fig. 7. Due to the change in EQE response with bias condition, one possible explanation for the loss in the long wavelength can be a reduced diffusion length in the PA sample, and particularly the multi-stack sample [27]. However, as can be seen in Fig. 5(b), the PA and multi-stack samples have slightly better PL decay time as compared to the REF. Thus, we can assume that the diffusion length of these samples is either similar to the reference or slightly better. This would indicate that the lowered diffusion length is not the reason for the observed changes. Rather, the change in the EQE response of the multi-stack sample under bias condition can be explained by assuming that added bias helps to reduce the effects created by the multi-stack oxide, and thus the carrier collection increases.

Another possible explanation of the deteriorated carrier collection (J_{sc} loss) in the long-wavelength region could be a

reduced space charge region (SCR) width [28]. Therefore, C-V measurements were performed on these samples to investigate if there is any change in doping level resulting in changed SCR width. The apparent doping concentration for each sample was extracted from the C-V measurement by using the Mott-Schottky plot in Fig.8(a). The apparent doping profiles are shown in Fig.8(b). As can be seen, the apparent doping increased dramatically with the addition of the NaCl pattern, leading to a reduction in the SCR width. This effect of sodium

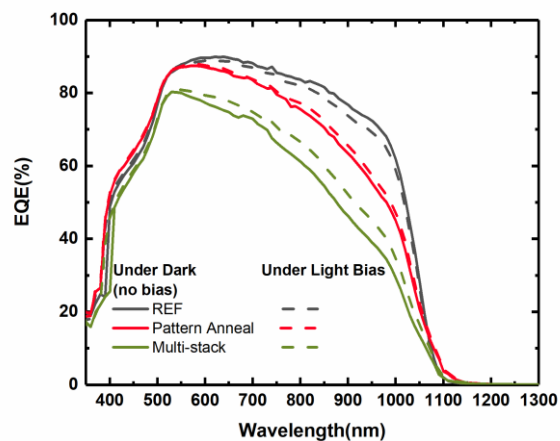


Fig. 7. The EQE spectrum under dark and light bias condition. Presence of the NaCl pattern in the sample leads the reduction in the long wavelength. A drop in the short wavelength was observed in the case of the multi-stack sample.

was already reported [28], [29]. Moreover, the apparent doping further increased, and the width of the SCR further reduced for the multi-stack sample. Since there was no additional treatment to the bulk except the addition of the multi-stack oxide layers for this sample, this behavior could be due to slightly different amount of the Na in the bulk. The PA sample was produced to distinguish between the effect of the oxide layer and NaCl pattern by mimicking the ALD process parameters. However, it is possible that the ALD deposition on the multi-stack sample and annealing condition of the PA sample are not exactly the same.

By analyzing both the EQE and C-V results, it can be said that the J_{sc} loss (i.e deteriorated carrier collection in the long wavelength) in the PA sample is most likely coming from the reduced SCR width. Due to the short diffusion length in the sample, the reduction of the SCR could not be compensated and the overall J_{sc} decreases. Moreover, it can be said that the multi-stack sample has an additional problem, besides the reduced SCR width, due to the negatively charged oxide layers with sub-optimal contacts. When these problems in the multi-stack design are combined with poor PL decay time, it leads to a more severe J_{sc} loss.

So far, we observed that the deteriorated device performance

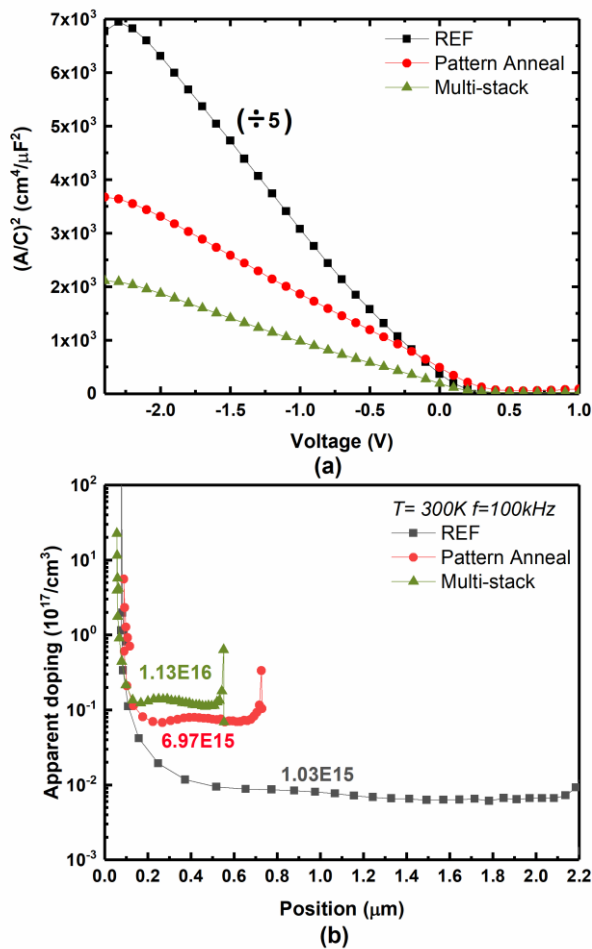


Fig. 8. (a) Mott-Schottky plot for each sample. The data of the REF sample was divided by 5 to create a readable graph. (b) Apparent doping profiles at 100kHz extracted from C-V measurement. The doping level increases, and space charge region width shrinks with NaCl addition (PA sample) and the multi-stack design compared to the reference sample.

is mainly coming from current loss in the multi-stack design. However, this loss is not coming only from the addition of the oxide layer but also the NaCl pattern itself. We believe that this loss in the current can be fixed by choosing a different oxide material and optimizing the contact opening pattern (i.e smaller and denser). Thus, this design could be beneficial even for a sample with short diffusion length. Yet, further investigation is needed to understand the behavior showcased by the PA and multi-stack samples. To avoid the problems observed in this study, it could be advantageous to use an absorber material with a longer average carrier diffusion length or alternatively prevent the interaction between the NaCl and the absorber material. Nevertheless, our approach showed promising results for the front interface applications for CIGS solar cells and we believe that when this novel multi-stack design is optimized further, or used with different combinations of oxides or alternative materials, it can be promising for future applications.

IV. CONCLUSION

In this contribution, we introduced a novel $\text{Al}_2\text{O}_3/\text{HfO}_2$ multi-stack design for front surface passivation of CIGS solar cells. The novelty of this process is that a non-chemically resistant material like Al_2O_3 is protected, using a thin HfO_2 layer, from an ammonia-based solution as found in chemical bath deposition processes. We showed that this approach is chemically resistant to the conventional chemical bath deposition by visualizing the openings via SEM and by confirming that both Al_2O_3 and HfO_2 layers survive after chemical deposition with EDS measurements. This approach allows us to keep the electronically favorable oxide/CIGS interface without impacting the standard processing of our solar cells. In addition, we showed that contact openings can be created effortlessly in thick multi-stack oxide layers. Furthermore, the multi-stack design showed improvement in PL intensity, PL decay time and V_{oc} . However, further electrical characterization showed J_{sc} losses. This cannot exclusively be attributed to our sub-optimal contact openings in the multi-stack design, since the PA sample also showed deteriorated carrier collection at the long-wavelength region. We believe that the current loss leading to a slightly lower device performance in the multi-stack design sample may be due to the narrow SCR and negative fixed charges in the multi-stack, leading to repelling of minority carriers at the front surface and causing the difficulty to collect. Nevertheless, this multi-stack design shows promising results to be used in front surface passivation for CIGS solar cells, especially in the absence of the bandgap grading at the front surface. The most important finding is that this multi-stack design strategy opens the door to the use of a wide variety of different oxide materials while continuing to use conventional solar cell processing routes. It allows us to select oxide materials with suitable interface properties more freely without having to consider additional adaptation of the processing.

ACKNOWLEDGMENT

This work received funding from the European Union's H2020 research and innovation program under grant agreement No. 715027.

REFERENCES

- [1] M. Nakamura, K. Yamaguchi, Y. Kimoto, Y. Yasaki, T. Kato, and H. Sugimoto, "Cd-Free Cu (In, Ga) (Se, S) 2 Thin-Film Solar Cell With Record Efficiency of 23.35%," *IEEE J. Photovoltaics*, vol. 9, no. 6, pp. 1863–1867, 2019.
- [2] G. M. Wilson *et al.*, "The 2020 photovoltaic technologies roadmap," *J. Phys. D. Appl. Phys.*, vol. 53, no. 49, 2020.
- [3] M. Ochoa, S. Buecheler, A. N. Tiwari, and R. Carron, "Challenges and opportunities for an efficiency boost of next generation Cu(In,Ga)Se₂ solar cells: Prospects for a paradigm shift," *Energy Environ. Sci.*, vol. 13, no. 7, pp. 2047–2055, 2020.
- [4] D. K. Simon, P. M. Jordan, I. Dimstorfer, F. Benner, C. Richter, and T. Mikolajick, "Symmetrical Al₂O₃-based passivation layers for p- and n-type silicon," *Sol. Energy Mater. Sol. Cells*, vol. 131, pp. 72–76, 2014.
- [5] G. Birant *et al.*, "Innovative and industrially viable approach to fabricate AlOx rear passivated ultra-thin Cu(In, Ga)Se₂ (CIGS) solar cells," *Sol. Energy*, vol. 207, no. April, pp. 1002–1008, 2020.
- [6] G. Birant *et al.*, "Rear surface passivation of ultra-thin CIGS solar cells using atomic layer deposited HfO_x," *EPJ Photovoltaics*, vol. 11, pp. 1–5, 2020.
- [7] B. Vermang, V. Fjällström, X. Gao, and M. Edoff, "Improved rear surface passivation of Cu(In,Ga)Se₂ solar cells: A combination of an Al₂O₃ rear surface passivation layer and nanosized local rear point contacts," *IEEE J. Photovoltaics*, vol. 4, no. 1, pp. 486–492, 2014.
- [8] S. Choi, Y. Kamikawa, J. Nishinaga, A. Yamada, H. Shibata, and S. Niki, "Lithographic fabrication of point contact with Al₂O₃ rear-surface-passivated and ultra-thin Cu(In,Ga)Se₂ solar cells," *Thin Solid Films*, vol. 665, no. January, pp. 91–95, 2018.
- [9] G. Sozzi, S. Di Napoli, R. Menozzi, B. Bissig, S. Buecheler, and A. N. Tiwari, "Impact of front-side point contact/passivation geometry on thin-film solar cell performance," *Sol. Energy Mater. Sol. Cells*, vol. 165, no. March, pp. 94–102, 2017.
- [10] A. Bercegol, B. Chacko, R. Klenk, I. Laueremann, M. C. Lux-Steiner, and M. Liero, "Point contacts at the copper-indium-gallium-selenide interface—A theoretical outlook," *J. Appl. Phys.*, vol. 119, no. 15, p. 155304, 2016.
- [11] W. W. Hsu *et al.*, "Surface passivation of Cu(In,Ga)Se₂ using atomic layer deposited Al₂O₃," *Appl. Phys. Lett.*, vol. 100, no. 2, pp. 1–4, 2012.
- [12] S. Garud *et al.*, "Surface Passivation of CIGS Solar Cells Using Gallium Oxide," *Phys. Status Solidi a*, vol. 1700826, pp. 1–6, 2018.
- [13] A. Hultqvist, T. Sone, and S. F. Bent, "Buffer Layer Point Contacts for CIGS Solar Cells Using Nanosphere Lithography and Atomic Layer Deposition," *IEEE J. Photovoltaics*, vol. 7, no. 1, pp. 322–328, 2017.
- [14] J. Löckinger *et al.*, "The use of HfO₂ in a point contact concept for front interface passivation of Cu(In,Ga)Se₂ solar cells," *Sol. Energy Mater. Sol. Cells*, vol. 195, no. January, pp. 213–219, 2019.
- [15] D. K. Simon, P. M. Jordan, T. Mikolajick, and I. Dimstorfer, "On the Control of the Fixed Charge Densities in Al₂O₃-Based Silicon Surface Passivation Schemes," *ACS Appl. Mater. Interfaces*, vol. 7, no. 51, pp. 28215–28222, 2015.
- [16] F. Werner, B. Veith-Wolf, M. Melchiorre, F. Babbe, J. Schimdt, and S. Siebentritt, "Ultra-thin passivation layer in Cu(In,Ga)Se₂ thin-film solar cells: full-area passivated front contacts and their impact on bulk doping," *Sci. Rep.*, vol. 10, no. 7530, 2020.
- [17] M. A. Curado *et al.*, "Front passivation of Cu(In,Ga)Se₂ solar cells using Al₂O₃: Culprits and benefits," *Appl. Mater. Today*, vol. 21, 2020.
- [18] J. Oh, J. Myoung, J. S. Bae, and S. Lim, "Etch Behavior of ALD Al₂O₃ on HfSiO and HfSiON Stacks in Acidic and Basic Etchants," *J. Electrochem. Soc.*, vol. 158, no. 4, p. D217, 2011.
- [19] J. De Wild *et al.*, "High Voc upon KF Post-Deposition Treatment for Ultrathin Single-Stage Coevaporated Cu(In, Ga)Se₂ Solar Cells," *ACS Appl. Energy Mater.*, vol. 2, no. 8, pp. 6102–6111, 2019.
- [20] D. G. Buldu *et al.*, "Study of Ammonium Sul fi de Surface Treatment for Ultrathin Cu (In, Ga) Se 2 with Different Cu/(Ga p In) Ratios," vol. 2000307, pp. 1–7, 2020.
- [21] D. G. Buldu *et al.*, "A multi-stack Al₂O₃/HfO₂ design with contact openings for front surface of Cu (In, Ga) Se₂ solar cells," in *48th IEEE Photovolt. Specialists Conf.*, 2021.
- [22] F. Pianezzi *et al.*, "Unveiling the effects of post-deposition treatment with different alkaline elements on the electronic properties of CIGS thin film solar cells," *R. Soc. Chem.*, vol. 16, pp. 8843–8851, 2014.
- [23] B. Chacko, "Point Contacts in Chalcopyrite Solar Cells," 2018.
- [24] S. Shirakata, K. Ohkubo, Y. Ishii, and T. Nakada, "Effects of CdS buffer layers on photoluminescence properties of Cu(In,Ga)Se₂ solar cells," *Sol. Energy Mater. Sol. Cells*, vol. 93, no. 6–7, pp. 988–992, 2009.
- [25] P. Reinhard *et al.*, "Alkali-templated surface nanopatterning of chalcoenide thin films: A novel approach toward solar cells with enhanced efficiency," *Nano Lett.*, vol. 15, no. 5, pp. 3334–3340, 2015.
- [26] R. Scaffidi *et al.*, "Comparative Study of Al₂O₃ and HfO₂ for Surface Passivation of Cu(In,Ga)Se₂ Thin-Films: An Innovative Al₂O₃/HfO₂ Multi-Stack Design," *Phys. Status Solidi*, vol. 2100073, pp. 1–8, 2021.
- [27] J. Keller *et al.*, "Heavy Alkali Treatment of Post-Sulfurized Cu(In,Ga)Se₂ Layers: Effect on Absorber Properties and Solar Cell Performance," *Sol. RRL*, vol. 4, no. 9, 2020.
- [28] C. Andres *et al.*, "Decoupling of optoelectronic properties from morphological changes in sodium treated kesterite thin film solar cells," *Sol. Energy*, vol. 175, no. February, pp. 94–100, 2018.
- [29] A. Urbaniak *et al.*, "Effects of Na incorporation on electrical properties of Cu(In,Ga)Se₂-based photovoltaic devices on polyimide substrates," *Sol. Energy Mater. Sol. Cells*, vol. 128, pp. 52–56, 2014.